Examples of Improved Inversion of Different Airborne Electromagnetic Datasets Via Sharp Regularization

Giulio Vignoli[1,2], Vincenzo Sapia[3], Antonio Menghini[4] and Andrea Viezzoli[4]
[1]Groundwater and Quaternary Geology Mapping Department, Geological Survey of Denmark and Greenland, C.F. Møllers Allé 8, DK-8000 Aarhus C, Denmark
[2]Dipartimento di Ingegneria Civile, Ambientale e Architettura, Università di Cagliari, via Marengo 2, 09123 Cagliari, Italia
Email: gv@geus.dk
[3]Istituto Nazionale di Geofisica e Vulcanologia, Via di Vigna Murata 605, 00143, Rome, Italy
Email: vincenzo.sapia@ingv.it
[4]Aarhus Geophysics Aps, C.F. Møllers Alle 4, Aarhus C 8000, Denmark
Emails: am@aarhusgeo.com; av@aarhusgeo.com

ABSTRACT

Large geophysical datasets are produced routinely during airborne surveys. The Spatially Constrained Inversion (SCI) is capable of inverting these datasets in an efficient and effective way by using a 1D forward modeling and, at the same time, enforcing smoothness constraints between the model parameters. The smoothness constraints act both vertically within each 1D model discretizing the investigated volume and laterally between the adjacent soundings. Even if the traditional, smooth SCI has been proven to be very successful in reconstructing complex structures, sometimes it generates results where the formation boundaries are blurred and poorly match the real, abrupt changes in the underlying geology. Recently, to overcome this problem, the original (smooth) SCI algorithm has been extended to include sharp boundary reconstruction capabilities based on the Minimum Support regularization. By means of minimization of the volume where, the spatial model variation is non-vanishing (*i.e.,* the support of the variation), sharp-SCI promotes the reconstruction of blocky solutions. In this paper, we apply the novel sharp-SCI method to different types of airborne electromagnetic datasets and, by comparing the models against other geophysical and geological evidences, demonstrate the improved capabilities of in reconstructing sharp features.

Introduction

Like almost all geophysical problems, the inversion of airborne electromagnetic data is ill-posed. Thus, because of the finite number of measurements, the unavoidable presence of noise in the data, and imperfect forward modeling, we observe that the inverse model solutions may vary largely as a consequence of small perturbations in the data (solution instability) and there may be many different models fitting the data equally well (solution non-uniqueness). In order to overcome these problems, the inclusion of a-priori geological information into the inversion process is essential. Historically, this has been done by enforcing a certain degree of smoothness. That is, among all the possible solutions compatible with the data, the smoothest one is chosen.

The smooth approach may produce suitable models in a sedimentary environment where material properties vary gradually. The justification for doing this is that the smooth solution is claimed to be the "simplest" according to the principle of Occam (Constable *et al*., 1987). In several cases, it has been shown that a smoothly varying parameter distribution is not necessarily simpler than a solution made of a few, homogenous domains (Last and Kubik, 1983). So in essence, it depends on what we mean by "simple", and our representation of the physical world has to be as simple as possible in order to be effective and practical (see, for example, Høyer *et al*., 2015a). The fact is that the majority of the geological interpretations of geophysical data consists of geological units with sharp boundaries. Therefore, in many cases, "simple" should be interpreted

 DOI: #10.2113/JEEG22.1.51

as "blocky". For these reasons, a series of focusing regularizations has been studied and implemented over the years to invert for the sharpest possible solution.

A way of requiring sharpness in the result is to look for the solution with the minimum number of model parameters with a non-vanishing spatial gradient, characterized by the minimum number of parameter values different from a reference model. These requirements can be quite easily implemented via the Minimum Gradient Support (MGS) and the Minimum Support (MS) stabilizers (Portniaguine and Zhdanov, 1999). It can be shown that once the "standard" smooth L2-norm algorithm is available, it is quite straightforward to implement its associated MGS and/or MS version (Zhdanov *et al*., 2006). These two focusing stabilization techniques have been successfully applied to a number of different geophysical problems. Examples of the applications on both seismic and radar travel-time tomography to enhance the resolution in the reconstruction of blocky targets can be found in Vignoli and Zanzi, (2005), Ajo-Franklin *et al.* (2007), and Vignoli *et al.* (2012). Concerning electrical resistivity and induced polarization tomography, the MGS/MS regularizations have been applied in space (Blaschek *et al*., 2005; Pagliara and Vignoli, 2006; Blaschek *et al.,* 2008) and time (Kim and Cho, 2011; Hermans *et al*., 2014; Fiandaca *et al*., 2015). In the latter case, the focusing stabilization techniques act between different stages in order to penalize results with models that, at different instants, are characterized by diffuse variations. Instead, they promote solutions with models that are equal almost everywhere except for the minimum number of model parameters necessary to fit the time-lapse data reasonably well (*i.e.,* within the noise level). Other successful applications of the MGS/MS regularization concern 2D/3D gravity and electromagnetic data (*e.g.,* Zhdanov, 2009).

In this paper, we discuss specifically airborne time-domain electromagnetic (ATEM) data. During airborne surveys, large quantities of electromagnetic data are collected. Full 3D inversion is possible (Cox *et al*., 2010; Ley-Cooper *et al*., 2015), but typically impractical as the Maxwell's equations need to be solved for each transmitter location making the rigorous 3D inversion expensive. Thus, seldom are 3D inversions performed and approaches based on 1D forward modeling are still routinely applied (Viezzoli *et al*., 2010). ATEM inversion codes based on 1D forward modeling typically use both vertical and lateral spatial constraints to regularize the inversion and obtain pseudo-3D solutions in accordance with the expected conceptual model. Other geophysical inversion methods, such as the Spatially Constrained Inversion (SCI) once implemented only the Occam-type regularization (Viezzoli *et al*., 2008). Within the smooth SCI framework, sharp petrophysical interfaces were retrieved merely by using a discretization with a limited number of layers (Auken and Christiansen, 2004). However, this "few-layer inversion" approach, in which the regularization is performed by means of the parameterization as well as the stabilization term acting only in the horizontal direction, is obviously very sensitive to the specific choice of the discretization and is prone to artifacts in case of unexpected complex geological structures. Recently, an extension of the SCI algorithm has been developed to include the possibility of sharp inversions via MGS and MS regularization (Vignoli *et al*., 2015a; Ley-Cooper *et al*., 2015).

In the present paper, after a short and practical description of the sharp-SCI, we discuss four examples of its application and compare these results against those obtained with smooth SCI and other diverse sources of information (*e.g*., geophysical log, existing geological maps, reflection seismic data). We show that in the appropriate conditions, the sharp SCI is superior to the smooth approaches in mapping sharp resistivity transitions and in facilitating geological interpretation (Vignoli *et al*., 2015b).

A Practical Introduction to the Methodology

In the inversion of airborne TEM datasets via 1D forward modeling, the models corresponding to adjacent soundings are often reciprocally constrained. The inversion problem is notoriously ill-posed and enforcing a certain level of entanglement between the models is a reasonable way of selecting the unique and stable solution in presence of quasi-layered structures when 2D or 3D effects are not pronounced (Newman *et al*., 1987; Sengpiel and Siemon, 2000; Auken *et al*., 2005). We refer to this approach as SCI and the entanglement between contiguous 1D models is provided by a lateral smoothing constraint term. In the case of a parametrization with numerous layers, this lateral constraint is associated with a similar term acting in the vertical direction. Hence, the SCI is a 2D/3D Occam inversion with a 1D forward model and it is characterized by all the advantages (and limitations) of this kind of regularization. For example, the SCI has been proven very effective (both in terms of quality of the final result and computational efficiency) in sedimentary settings where the regularization assumption is clearly met (Jørgensen *et al*., 2012; Jørgensen *et al*., 2013; Schamper

et al., 2014). On the other hand, the smooth SCI generates 2D/3D models where formation boundaries may appear smeared.

In the attempt to reconstruct sharp features with high detail, a sharp SCI algorithm has been developed. In the sharp SCI, the lateral and vertical regularization terms are not defined as the L2-norm of the gradient of the solution, but as its gradient support (Vignoli *et al*., 2015a). By gradient support we mean the number of model parameters where the gradient is non-vanishing. In using the sharp version of the SCI, we search for the solution characterized by the minimum number of lateral and vertical spatial variations instead of the solution with the minimum spatial variation that is a characteristic of the smooth SCI.

The standard SCI consists of finding the minimum of the objective function representing the sum of the data misfit $\phi(\mathbf{m})$ and the stabilizer (s) is:

$$s^{(smooth\ SCI)}(\mathbf{m}) = \sum_k \frac{(\Delta\mathbf{m})_k^2}{\sigma_k^2}, \tag{1}$$

Equation 1 is the squared L_2-norm of the variation of the model parameters $\Delta\mathbf{m}$, with the variation components weighted by the model variance σ_k. In the specific case we are considering here, the components of model vector $\mathbf{m}$ contains the resistivity values of the layers, while σ_k represents the degree of spatial variability of the solution. Hence, the larger the weighted variations of the model parameters, the higher the stabilizer value (and so the corresponding penalization). However, there is no differentiation between small and large contributions from each addendum in Eq. 1. Not discriminating between small and large contributions prevents the possibility of the reconstruction of blocky structures.

In the sharp SCI, we substitute the stabilizing term with:

$$s^{(sharp\ SCI)}(\mathbf{m}) = \sum_k \frac{\left(\frac{(\Delta\mathbf{m})_k}{\sigma_k}\right)^2}{\left(\frac{(\Delta\mathbf{m})_k}{\sigma_k}\right)^2 + 1}. \tag{2}$$

The sharp stabilizer counts the number of variations larger than the σ_k values (Vignoli *et al*., 2015a). Hence, by minimizing the objective function with the focusing stabilizer described in Eq. 2, we are selecting, amongst all the possible solutions compatible with the data, the one that has the minimum number of model variations larger than the threshold defined by σ_k. So, σ_k acts as a measure of the variability tolerated within a formation to be considered homogeneous. Variations smaller than that are weakly penalized in a way that is similar to the smooth regularization. Variations larger than the threshold equally contribute to the summations in Eq. 2, and it does not really matter if they are small or large (as long as they are larger than σ_k).

Following the standard Tikhonov's formalism, in the objective function to be minimized, the term in Eq. 2 is weighted by an additional coefficient. In Vignoli *et al*. (2015a), the additional coefficient is called β^{-1} and it is responsible for controlling the relative importance between the data and the regularization. Hence, the objective function to be minimized during the inversion is:

$$\phi(\mathbf{m}) + (1/\beta)\ \ s(\mathbf{m}) \tag{3}$$

where $\phi(\mathbf{m})$ is the L_2-distance between the calculated and observed data, and $s(\mathbf{m})$ is the stabilizing term as defined in either Eq. 1 or Eq. 2. The coefficient β should be selected as small as possible, but still allowing the algorithm to reach the desired level of data misfit. In this way, the importance of our a-priori knowledge (in this case geometric with the presence of smooth or sharp transitions) formalized by the stabilizer $s(\mathbf{m})$ is chosen to be the largest possible without overriding the information from the data.

Field Examples

In this section, we present the results from three different AEM systems. The first is a test conducted on a TEMPEST dataset from Western Australia demonstrating the enhanced capability of the sharp inversion in retrieving the geological structures, compared to the information from a geophysical log. The second test models a VTEM dataset collected in the Spiritwood Valley Aquifer area, Manitoba, Canada. This dataset was chosen because of previous extensive studies in the area (*e.g*., Oldenborger *et al*., 2013) and the simultaneous availability of reflection seismic data along many of the flight lines (Sapia *et al*., 2014). For these reasons, it has been possible: 1) to assess the agreement between the sharp SCI results and the other kind of geophysical data and 2) to evaluate the match with former geological investigations. The last example consists of an Aero-TEM dataset, also acquired in the Spiritwood area, which makes evident how different the inversion results could be by simply selecting different a-priori geometric information.

Paterson Survey

The first example concerns a TEMPEST dataset collected in the Paterson area of Western Australia. The data are available online and can be freely downloaded

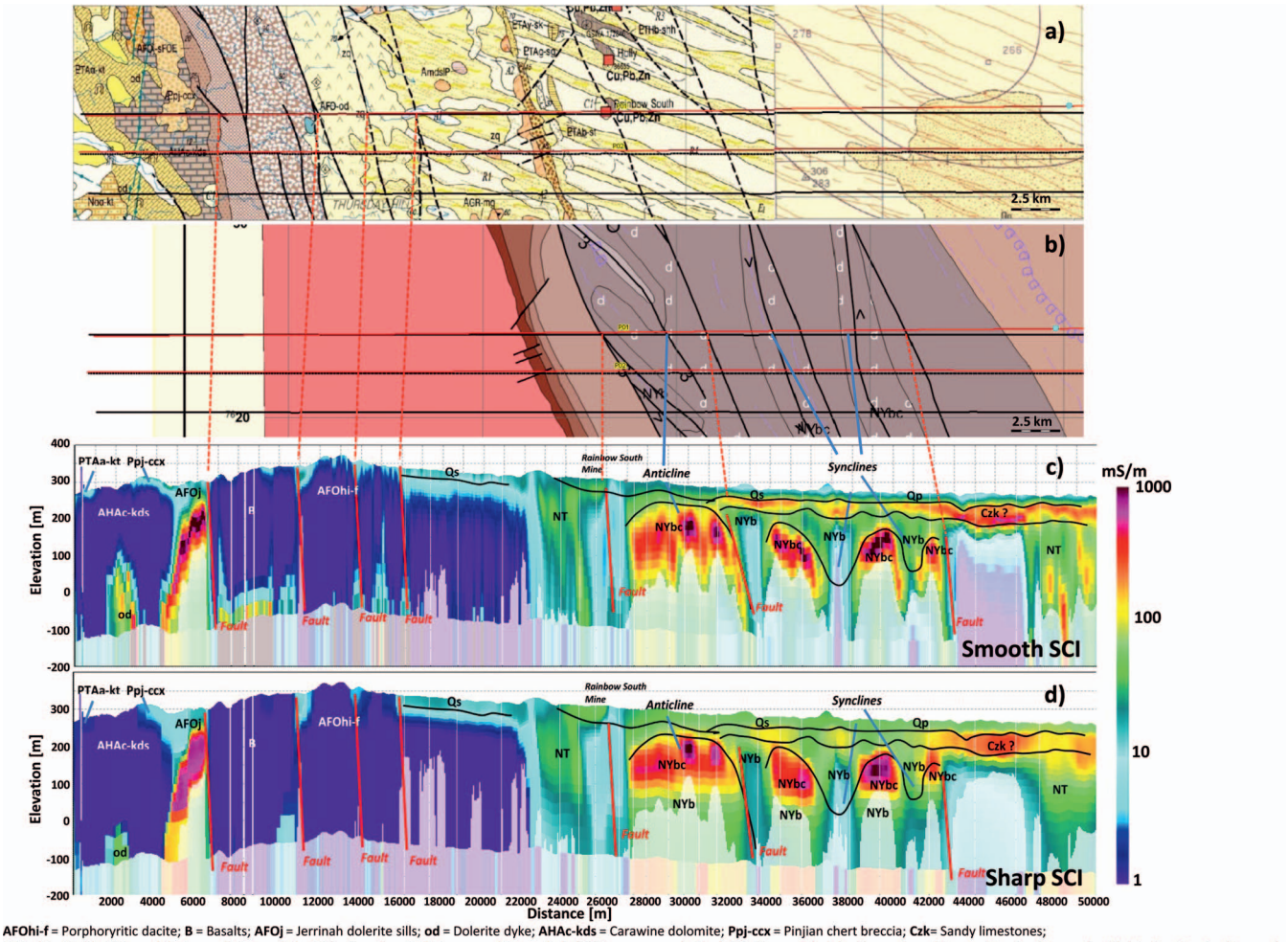

AFOhi-f = Porphoryritic dacite; **B** = Basalts; **AFOj** = Jerrinah dolerite sills; **od** = Dolerite dyke; **AHAc-kds** = Carawine dolomite; **Ppj-ccx** = Pinjian chert breccia; **Czk**= Sandy limestones; **PTAa-kt** = Waltha Woora dolostone, siltstone, shale; **NYb**= Broadhurst siltstone, sandstone, shale (**NYBc**= more conductive); **NT**= Tarcunyah dolomites and sandstones; **Qp**= Aeolian sands with laterite; **Qs**= Aeolian sands.

Figure 1. Paterson survey (TEMPEST data), L30760. a) Geological map (sheets SF 51-6 Paterson Range and SF 51-5 Nullagine, scale 1:250.000); b) Bedrock geology map (Proterozoic solid geology of the Paterson area, scale 1:250.000); c) Smooth SCI inversion (29 layers); d) Corresponding sharp-SCI. Respectively, the dashed red and solid blue lines connect the faults, and the anticline/synclines axes in the geological maps to those resolved by the airborne electromagnetic inversions. The geological codes of the various formations are at the bottom of the panel (d).

from the Geoscience Australia website: http://www.ga.gov.au/metadata-gateway/metadata/record/gcat_70297. TEMPEST is a fixed-wing time-domain system that employs an approximate square-wave 50% duty cycle current waveform with a base frequency of 25 Hz. The current is transmitted through a single turn transmitter (TX) loop draped around the nose, wings, and tail of the aircraft. The survey was flown with the TX loop at 122.4 m above ground level on average. The receiver (RX) coils is housed in a 'bird' that is towed at approximately 120 m behind and 35 m below the aircraft. The RX consisted of three orthogonal coils that sense the rate of change of the magnetic field (dB/dt) flux threading each coil. We processed both X and Z-component, inverting also for the actual vertical and horizontal offset between Tx and Rx. Further details on TEMPEST can be drawn from Lane *et al*. (2000).

Figures 1(a) and (b) show the outcropping geology (sheet SF 51-6 Paterson Range) and the Proterozoic bedrock geology as it was retrieved on the basis of outcrop geology, drilling information, aeromagnetic data, gravity, and ground electromagnetics. For the inversion of the airborne data, the parameterization consisted of 29 layers, ranging from 3 and 400 m depth, having thickness logarithmically increasing with depth. The results of a subset of the data (L30760) are presented in Figs. 1(c) and (d). It is worth highlighting that the profile is 50 km long. The vertical exaggeration is more than a factor of ten and may influence the perception of the lateral variations.

The smooth inversion (Fig. 1(c)) is capable of resolving many geological and structural features. Firstly, the response of the strongly resistive Archean basement is completely different from the Proterozoic sediments, which are more conductive. In addition, the dolerite dyke alignment ("od") in the geological map (blue line with dots in Fig. 1(a)) is well imaged as a vertical conductive structure within the resistive Carawine dolomite ("AHAc-kds"), basalts ("B"), and porphoryritic dacite ("AFOhi-f"). In addition, the Jerrinah dolerite sill ("AFOj") seems connected with a nearly vertical conductive feature. Within the Archean complex on the left, at least four faults mapped by the geological survey are well resolved by the resistivity contrast on the shallower section.

Starting from distance 16,000 m in the profile, we enter into the Quaternary deposits composed by Aeolian sands ("Qs" and "Qp") that mask the Proterozoic complex. Thus, the bedrock geology map (Fig. 1(b)) is more useful to interpret the geophysical data. The excellent agreement between the axis of synclines and anticlines inferred by the Geological Survey of Western Australia is remarkable. The dashed red and continuous blue lines connect the faults and the anticline/synclines axes of the geological maps to those resolved by airborne EM. This result was possible because of the strong conductive response of the top layers of the Broadhurst formation ("NYbc").

The corresponding sharp SCI results are shown in Fig. 1(d). As expected, the reconstruction of the electrical conductivity distribution is sharper compared with the smooth profile in Fig. 1(c). The sharp model allows for an easier geological interpretation of the petrophysical features and structures. For example, the dyke and the faults crossing the basement on the left side of the profile, as well as the contact among the formations on the right side, are better resolved and more clearly highlighted. The higher resolution of contacts makes for more a straightforward match between the geological maps and the geophysical results. The sharp SCI model is also capable of providing compact resistivity structures separated by clear contacts. This, in turn, makes all picking operations, which are the first step of any geological modeling, easily facilitated. For example, the top of the resistive basement between 16,000 and 22,000 m is better defined. The same is true for the dyke at around 2,000 m and the dolerite sill near 6,000 m. In these cases, the sharp reconstruction consists of very homogeneous blocks of 20 and 800 mS/m, respectively. Compared with the smooth result, the sharp SCI model allows for more certain and easily identifiable structures and detection of their boundaries. Similarly, the sharp SCI reconstruction of the anticlines appears more blocky without the lateral variability evident in the smooth result.

Concerning the detection of the faults, the sharp inversion is more effective in most parts of the model because of its homogeneous reconstruction of the different geological units. The sharp model more precisely locates these features due to the clearer evidences in the shallow portion within the Archean complex. On the contrary, faults appear to be easier to see in the smooth solution on the right side of the section. The reason is that the sharp inversion, with resistive bodies interpreted as anticlines, are more compact and shallower. Nevertheless, it is worth noticing that the sharp and smooth inversions provide significantly different results at depth, and well above the calculated Depth of Investigation (DOI) using the approach outlined in Christiansen and Auken (2012). This, together with the fact that the two results fit the data equally well, makes questionable the validity of the present assessment of the DOI. Hence, a more reasonable estimation of the maximum depth at which the results could be considered effectively constrained by the data should be probably shallower.

Figure 2 shows a comparison of the smooth and sharp 1D inverse models with corresponding borehole results. In the electrical conductivity log, shown as the black line in Fig. 2(b), the abrupt conductivity change between the different facies of the Broadhurst formation is evident: "NYb" is characterized by a conductivity of around 0.04 S/m, while "NYbc" has values of about 0.5 S/m. Figures 2(a) and (c) show the 1D inversion results extracted from the smooth and sharp profiles, respectively. Figure 2(b) shows the geophysical log along with a third inversion method called the Layered Earth Inversion, performed by Geoscience Australia (Lane *et al*., 2004); we call this GA-LEI. The resistivities inferred by the airborne data show the petrophysical variation associated with the transitions between "NYb" and "NYbc". However, the sharp result more precisely locates the boundaries of the "NYbc" facies, while the smooth SCI and the GA-LEI tend to smear the "NYbc-NYb" interfaces and lowering their positions. In conclusion, the sharp model is capable of resolving the "NYbc" layer better, both in terms of conductivity values and of depth and thickness, proving its effectiveness against the more standard approaches. On the other hand, smaller resistivity oscillations, evident in the log in the first 100 m, are flattened out by the sharp inversion.

We can further assess the advantages of the sharp inversion against the corresponding smooth model by

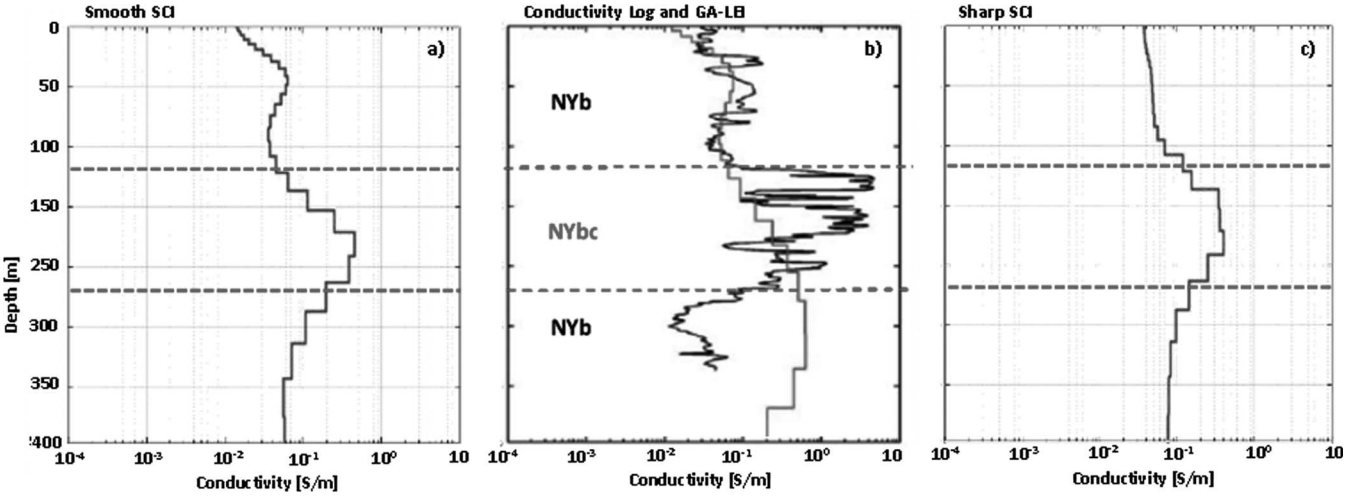

Figure 2. Data from the Paterson survey. a) 1D conductivity model obtained with the traditional, smooth SCI regularization; b) Conductivity borehole log (solid black line) and 1D conductivity model using GA-LEI; c) 1D conductivity model obtained with the sharp regularization (sharp SCI). The dashed horizontal lines show the top and the bottom of the "NYbc" facies as inferred by the electrical conductivity log in panel (b).

studying the profile showed on Fig. 3. In fact, only the sharp regularization is capable of accurately imaging the fault system that interrupts the Jarlemai siltstone ("Js"). These faults can be confirmed by geological data. On the contrary, the smooth inversion resolves these tectonic features more poorly, as the model produces a nearly continuous layer. Similarly, the sharp inversion enhances the resolution in the reconstruction of the shallower

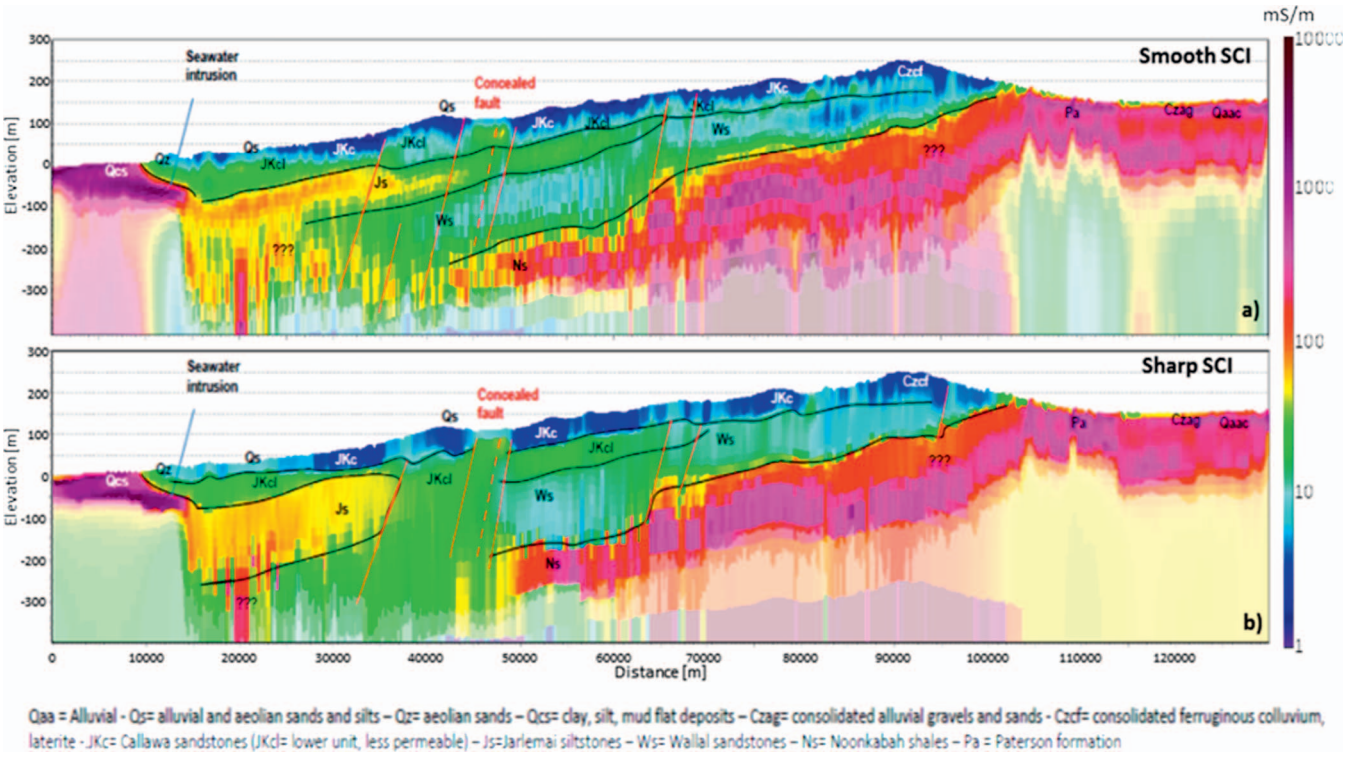

Figure 3. Paterson survey (TEMPEST data), L300082. a) Smooth SCI inversion with 29 layers; b) The corresponding sharp SCI result. The black and red, solid and dashed lines represent the geological interpretations based on the corresponding geophysical inversions. The geological codes of the various formations are shown at the bottom of the figure.

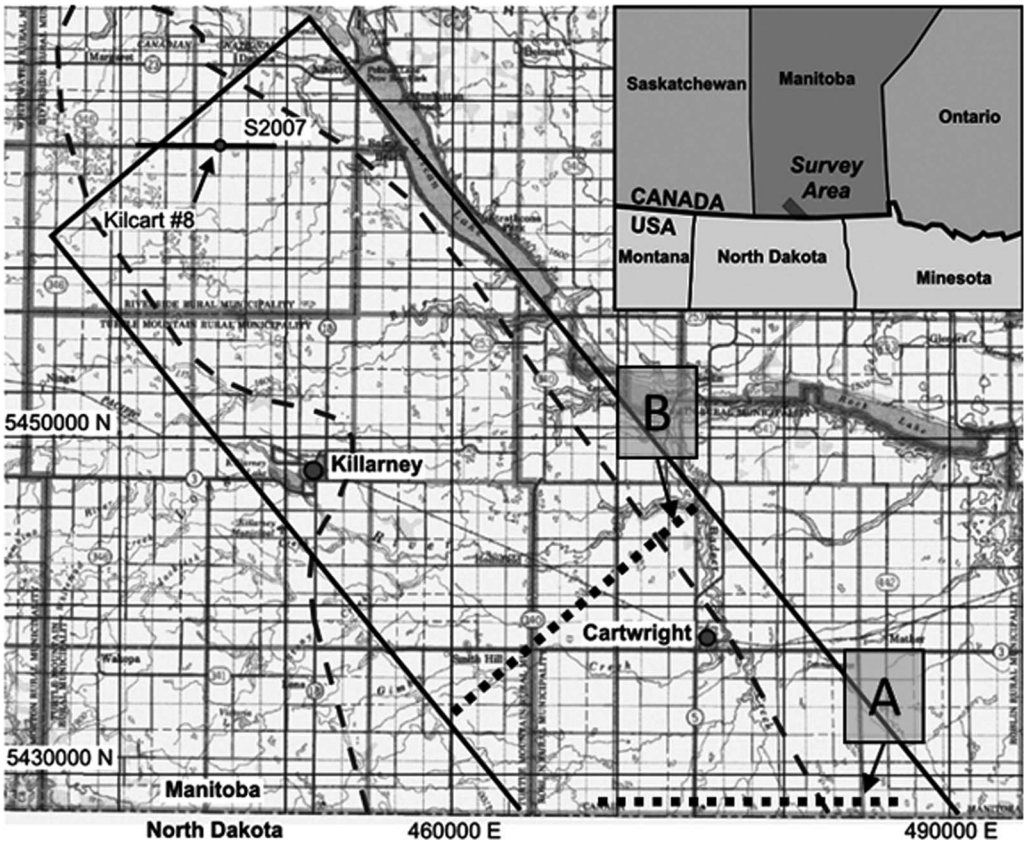

Figure 4. The Spiritwood survey area (solid black line). The dashed rectangles, indicated with A (VTEM) and B (AeroTEM), show the locations of the profiles discussed in the paper.

Callawa sandstone ("JKc") and of the top of Noonkabah shales ("Ns"), progressively dropping towards the left side of the profile by means of direct faulting. Maybe, analogous results could have been achieved by using fewer layers in the inversion (Auken *et al*., 2008). The risk, however, would likely have manifest as modeling artifacts due to fitting too few parameters to a very complex geological system.

Spiritwood Valley: VTEM Survey

The second example is based on a VTEM prospection (Fig. 4, profile A) over the Spiritwood Valley Aquifer. The Spiritwood Valley Aquifer is a Canada-USA trans-border buried valley aquifer that runs approximately NW–SE and extends 500 km from Manitoba, across North Dakota and into South Dakota (Winter *et al*., 1984). This aquifer consists of glacially deposited silt and clay diamicton with sand and gravel bodies, infilling a broad north-south trending shale bedrock valley and a series of narrow incised buried valleys (Oldenborger *et al*., 2013). Figure 5 shows a schematic of the geological setting of the area (Cummings *et al*., 2012). In 2011, Geotech performed a helicopter-borne geophysical survey over an area chosen as a "test area" based also on the availability of previous electrical and seismic data. VTEM data were collected using a newly developed system designed to improve early-time data and shallow imaging capability (Legault *et al*., 2012). Forty-four time-gates were used for final data processing, ranging from approximately 20 μs after current turn-off up to 10 ms for the late-time gates. At a later stage, the original data went through a sophisticated recalibration procedure to gain consistency with the ground-based measurements. The details of this recalibration can be found in Sapia *et al*. (2014). However, in the present research, we are more interested in investigating the advantages and opportunities provided by the different inversion schemes, and we are showing and discussing the results obtained before that recalibration.

The results obtained from inverting these data are displayed in Fig. 6. The smooth SCI result (Fig. 6(a)) is significantly different from the corresponding model obtained by using the sharp inversion (Fig. 6(c)). Additionally, it is clear that the sharp inversion is in agreement with the seismic information (Fig. 6(b)). For

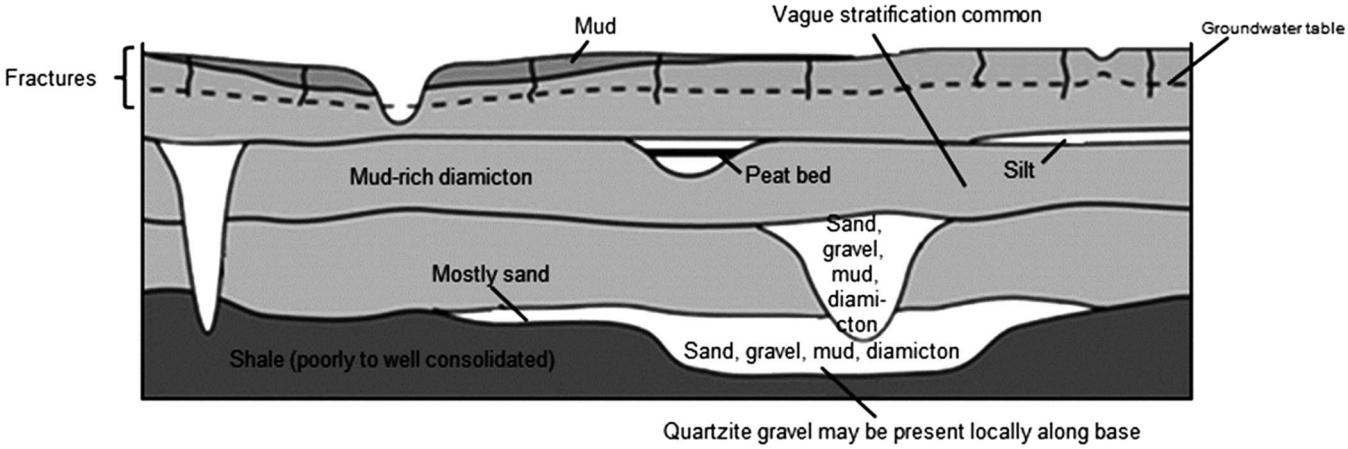

Figure 5. Schematic lithostratigraphy of the buried valleys in the Canadian Prairies (after Cummings et al., 2012).

example, subtle seismic features (*e.g.,* in the portion between 350 m and 400 m in elevation) are more easily readable after the comparison with sharp ATEM profile (Fig. 6, red lines). In addition, the horizontal layer, corresponding to the main reflector at around 400 m in the seismic profile, is smeared in the smooth inversion. On the other hand, the same interface is more clearly detected for a large portion of the profile by the sharp SCI model (Figs. 6(b) and (c)). The sharp inversion also more precisely locates the top of the gravel unit. This more resistive structure, filling up the bottom of the deeper valley, is highlighted by an intense reflection before the distance 9,000 m, and is confirmed by borehole information as characterized by a distinct interface between tills and gravels at a depth of approximately 80 m.

Spiritwood Valley: AeroTEM Survey

Numerous datasets have been collected over the Spiritwood area (Oldenborger, 2010a, 2010b; Crow *et*

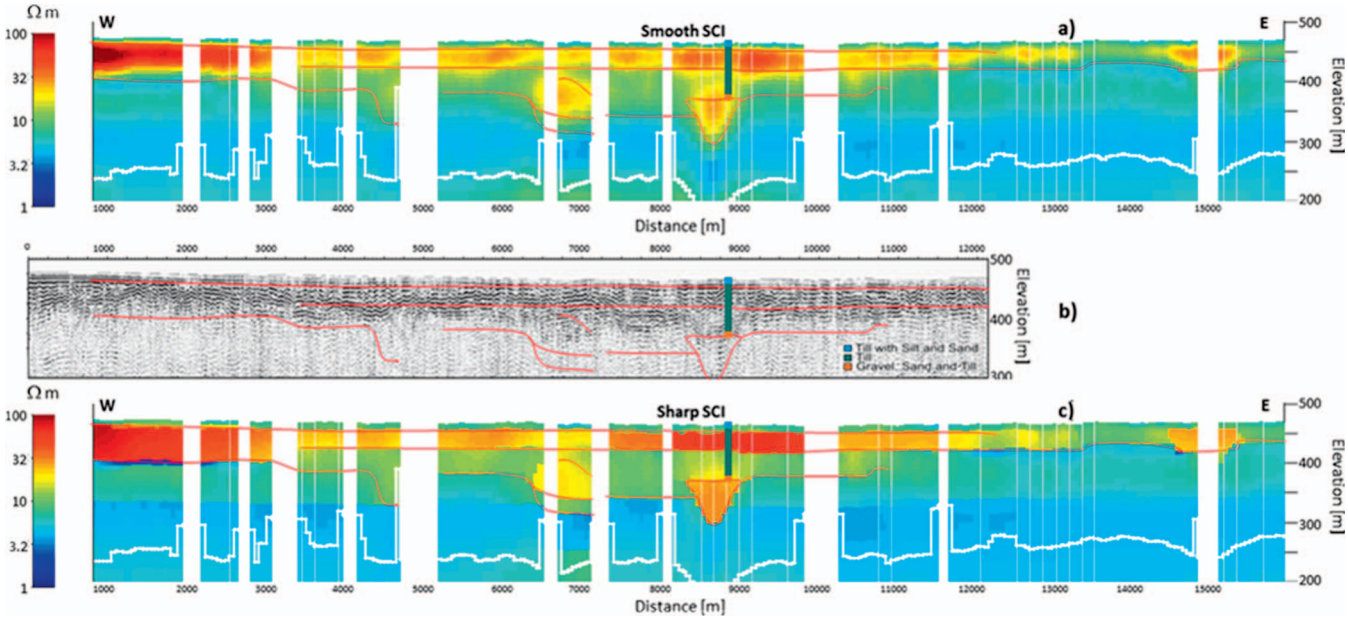

Figure 6. Spiritwood survey, profile A (VTEM data) from Fig. 4. a) The result from the smooth inversion of the airborne electromagnetic data together with the highlighted features derived from the sharp inversion. b) Comparison of the sharp result with the reflection seismics collected along the same line. c) The result obtained via the sharp SCI regularization. The red lines highlight the features for further comparison against the seismic and smooth results. The white solid lines in (a) and (c) represent the Depth of Investigation (DOI). In all the panels, the lithostratigraphy derived from borehole observations is shown.

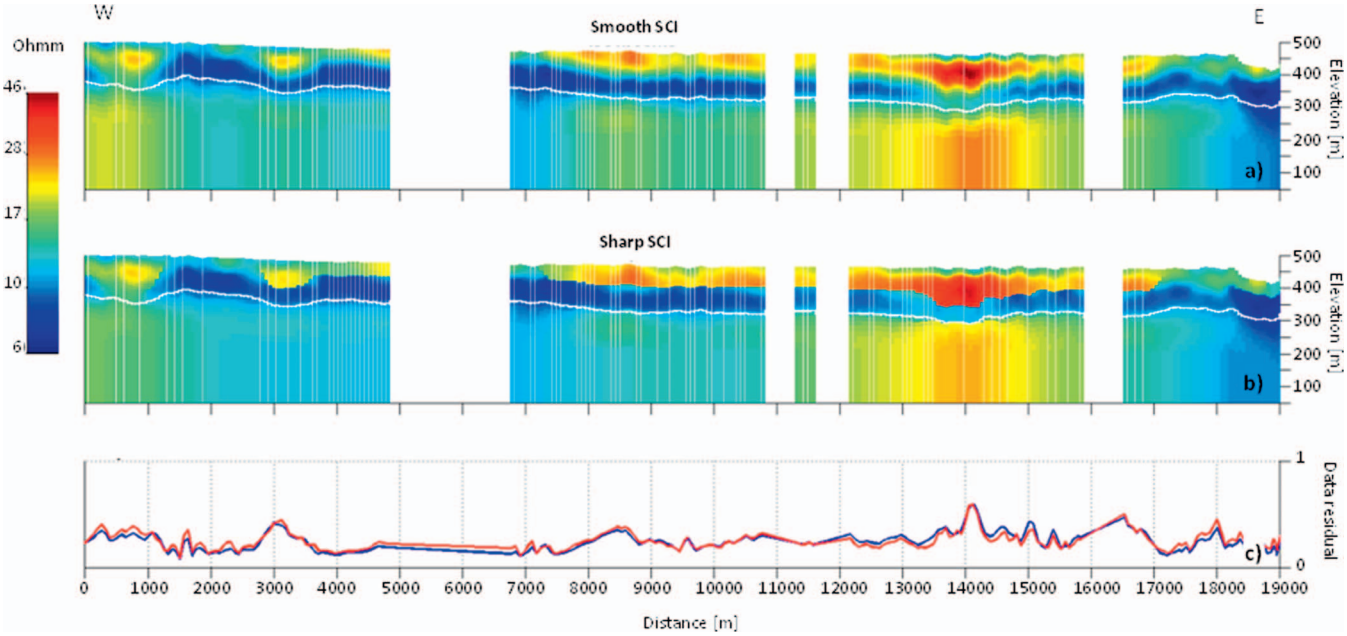

Figure 7. Spiritwood survey, profile B (AeroTEM data) in Fig. 4. a) Result obtained via the traditional smooth regularization applied to airborne electromagnetic data; b) the corresponding sharp inversion result; c) the associated data residuals (in blue the data misfit from the smooth inversion, in red the one generated by the sharp regularization). The white solid lines in (a) and (b) represent the Depth of Investigation (DOI).

al., 2012) making it a good candidate for survey comparisons. During 2010, before the VTEM data acquisition discussed above, the Geological Survey of Canada conducted an airborne electromagnetic (AeroTEM III) survey over 1,062 km^2 in the same area along the Spiritwood Valley, north of the US border. Our third example is based on one of those flight lines shown as profile B in Fig. 4. The data consist of seventeen off-time gates (70 μs to 3 ms after time-off). Before the inversion, the raw data were stacked, compensated, drift corrected, microlevelled, and cross-calibrated as discussed in Sapia *et al*. (2015a). We use this last example to highlight once more that when we compare smooth and sharp results, they are both equally compatible with the data. This means that they equally fit the data to the same desired level. The only difference between the smooth and sharp results is that they are also consistent with different a-priori information derived from our existing geological understanding. This a-priori information is incorporated into the inversion through the stabilizer term $s(\mathbf{m})$ from Eqs. 1 and 2. By looking the two results in Fig. 7, we can see how the data residuals of the two inversions are almost equal everywhere. The data misfits (Fig. 7(c)) are about the same, not only globally for the entire profile, but also locally for each individual sounding. Still, the smooth and sharp results are extremely different. The differences in model outcomes demonstrate the inherent ambiguity of the inversion at every scale, and the necessity of incorporating the appropriate geological knowledge into the process. By including the correct a-priori information (*i.e.,* the existence of sharp transitions between layers), we can retrieve the boundaries of the buried valleys and the continuity of the conductive layer in which they are embedded, with a resolution much higher than the one we observe when we apply the traditional smooth stabilizer. This paves the road, not only to the possibility of a faster cognitive geological interpretation of the geophysics (Høyer *et al*., 2015b; Sapia *et al*., 2015b), but also to the practical use of semi-automatic strategies for doing that (Gulbrandsen *et al*., 2015).

Conclusions

In this paper, we discuss a few examples of the application of the novel sharp SCI to several airborne TEM datasets. We compare these results against the corresponding models obtained with the standard, smooth SCI and against other geological and geophysical data. From these comparisons, it is clear that sharp SCI provides results with higher resolution of blocky petrophysical features. It is worth stressing that sharp SCI provides "better" results only when abrupt changes of the physical properties are expected. The sharp regularization simply incorporates in the inversion

process the geometrically based a-priori information we have about the target (*i.e.,* the existence of clear interfaces). For the same reason, whenever the resistivity distribution is smoothly varying, the sharp SCI will provide an erroneous blocky model honoring the data within the noise level. In these cases, the traditional smooth SCI would definitely provide a result closer to the reality. Thus, a regularization that is good in all cases does not exist; for each dataset, it is necessary to select/design the proper regularization consistent with the available a-priori information. Of course, in many cases, the sharp regularizations are the most correct and effective choices.

From the discussion in this paper, it is evident that the sharp SCI could potentially substitute the so-called few-layer inversion. For example, in the case of sharp SCI, there is no need for the troublesome choice of a unique few-layer parameterization to be used in the entire survey that may generate artifacts when facing unexpected geological complexities. In addition, the fact that the sharp reconstructions are, in many cases, closer to our geological representations is an advantage in terms of facilitating the geological interpretation of the geophysics. Potentially, this could promote the concrete use of semi-automatic strategy for the geological modeling based on the TEM data.

The sharp regularization approach is very general and easy to be implemented on top of any available L2-norm (smooth) algorithm. It has been applied to the inversion of many other data types including time-lapse DC resistivity, Induced Polarization, MRS, and traveltime tomography. In particular, with the evident similarities between TEM and seismic surface wave methodologies (Vignoli *et al*., 2016) we would expect that examples of applications of the sharp SCI to these seismic data will be available soon.

Acknowledgements

The Spiritwood AeroTEM data set is freely available from Natural Resources Canada. We thank Geotech Ltd. for provision of the VTEM data set. We are grateful to A. Pugin from the Geological survey of Canada for providing the seismic data. We would like to thank Geoscience Australia to allow us to work and publish their data. We also acknowledge and thank the reviewers Jeff Gamey and Andi A. Pfaffhuber for helpful comments and suggestions.

References

Auken, E., and Christiansen, A.V., 2004, Layered and laterally constrained 2D inversion of resistivity data: Geophysics, **69**, 752–761.

Auken, E., Christiansen, A.V., Jacobsen, B.H., Foged, N., and Sørensen, K.I., 2005, Piecewise 1D laterally constrained inversion of resistivity data: Geophysical Prospecting, **53**, 497–506.

Ajo-Franklin, J.B., Minsley, B.J., and Daley, T.M., 2007, Applying compactness constraints to differential traveltime tomography: Geophysics, **72**, R67–R75.

Blaschek, R., Hördt, A., and Kemna, A., 2005, A new regularization for the inversion of IP data based on the minimum gradient support: *in* Near Surface: 11th European Meeting of Environmental and Engineering Geophysics, 270–275.

Blaschek, R., Hördt, A., and Kemna, A., 2008, A new sensitivity-controlled focusing regularization scheme for the inversion of induced polarization data based on the minimum gradient support: Geophysics, **73,** F45–F54.

Constable, S., Parker, R., and Constable, C., 1987, Occam's inversion: A practical algorithm for generating smooth models from electromagnetic sounding data: Geophysics, **52**, 289–300.

Crow, H.L., Knight, R.D., Medioli, B.E., Hinton, M.J., Plourde, A., Pugin, A.J.M., Brewer, K.D., Russell, H.A.J., and Sharpe, D.R., 2012, Geological, hydrogeological, geophysical, and geochemistry data from a cored borehole in the Spiritwood buried valley, southwest Manitoba: *in* Geological Survey of Canada: Open file 7079.

Cox, L., Wilson, G., and Zhdanov, M.S., 2010, 3D inversion of airborne electromagnetic data using a moving footprint: Exploration Geophysics, **41**, 250–259.

Christiansen, A.V., and Auken, E., 2012, A global measure for depth of investigation: Geophysics, **77**, WB171–WB117.

Cummings, D.I., Russell, H.A.J., and Sharpe, D.R., 2012, Buried-Valleys in the Canadian Prairies: geology, hydrogeology, and origin: Canadian Journal of Earth Sciences, **49**, 987–1,004.

Gulbrandsen, M.L., Bach, T., Cordua, K.S., and Hansen, T.M., 2015, Localized Smart Interpretation - a data driven semi-automatic geological modelling method: *in* Extended Abstracts: 24th International Geophysical Conference and Exhibition, ASEG, 1–4.

Fiandaca, G., Doetsch, J., Vignoli, G., and Auken, E., 2015, Generalized focusing of time-lapse changes with applications to direct current and time-domain induced polarization inversions: Geophysical Journal International, **203**, 1101–1112.

Hermans, T., Nguyen, F., Robert, T., and Revil, A., 2014, Geophysical methods for monitoring temperature changes in shallow low enthalpy geothermal systems: Energies, **7**, 5083–5118.

Høyer, A.-S., Jørgensen, F., Sandersen, P.B.E., Viezzoli, A., and Møller, I., 2015a, 3D geological modelling of a complex buried valley network delineated from borehole and AEM data: Journal of Applied Geophysics, **122**, 94–102.

Høyer, A.-S., Jørgensen, F., Foged, N., He, X., and Christiansen, A.V., 2015b, Three-dimensional geological modelling of AEM resistivity data - A comparison of three methods: Journal of Applied Geophysics, **115**, 65–78.

Jørgensen, F., Scheer, W., Thomsen, S., Sonnenborg, T.O., Hinsby, K., Wiederhold, H., Schamper, C., Burschil, T., Roth, B., Kirsch, R., and Auken, E., 2012, Transboundary

geophysical mapping of geological elements and salinity distribution critical for the assessment of future sea water intrusion in response to sea level rise: Hydrology and Earth System Sciences, **16**, 1845–1862.

Jørgensen, F., Møller, R., Nebel, L., Jensen, N.-P., Christiansen, A.V., and Sandersen, P.B.E., 2013, A method for cognitive 3D geological voxel modelling of AEM data: Bulletin of Engineering Geology and the Environment, **72**, 421–432.

Kim, K.J., and Cho, I.K., 2011, Time-lapse inversion of 2D resistivity monitoring data with a spatially varying cross-model constraint: Journal of Applied Geophysics, **74**, 114–122.

Lane, R., Green, A., Golding, C., Owers, M., Pik, P., Plunkett, C., Sattel, D., and Thorn, B., 2000, An example of 3D conductivity mapping using the TEMPEST airborne electromagnetic system: Exploration Geophysics, **31**, 162–172.

Lane, R., Brodie, R., and Fitzpatrick, A., 2004, A revised inversion model parameter formulation for fixed wing transmitter loop-towed bird receiver coil time-domain airborne electromagnetic data: *in* Extended Abstract: 17th Geophysical Conference and Exhibition, ASEG.

Last, B.J., and Kubik, K.,1983, Compact gravity inversion: Geophysics, **48**, 713–721.

Legault, J.M., Prikhodko, A., Dodds, D.J., Macnae, J.C., and Oldenborger, G.A., 2012, Results of recent VTEM helicopter system development testing over the Spiritwood Valley aquifer, Manitoba: *in* Expanded Abstracts: 25th Symposium on the Application of Geophysics to Engineering and Environmental Problems, EEGS, 17.

Ley-Cooper, A.Y., Viezzoli, A., Guillemoteau, J., Vignoli, G., Macnae, J.C., Cox, L., and Munday, T., 2015, Airborne electromagnetic modelling options and their consequences in target definition: Exploration Geophysics, **46**, 74–84.

Newman, G.A., Anderson, W.L., and Hohmann, G.W., 1987, Interpretation of transient electromagnetic soundings over three-dimensional structures for the central-loop configuration: Geophysical Journal of The Royal Astronomical Society, **89**, 889–914.

Oldenborger, G.A., 2010a, AeroTEM III Survey, Spiritwood Valley, Manitoba, parts of NTS 62G/3, 62G/4, Manitoba: Geological Survey of Canada, Open File 6663.

Oldenborger, G.A., 2010b, AeroTEM III Survey, Spiritwood Valley, Manitoba, parts of NTS 62G/3, 62G/4, 62G/5, 62G/6, Manitoba: Geological Survey of Canada, Open File 6664.

Oldenborger, G., Pugin, A.J.M., and Pullan, S.E., 2013, Airborne time-domain electromagnetics, electrical resistivity and seismic reflection for regional three-dimensional mapping and characterization of the Spiritwood Valley Aquifer, Manitoba, Canada: Near Surface Geophysics, **11**, 63–74.

Pagliara, G., and Vignoli, G., 2006, Focusing inversion techniques applied to electrical resistance tomography in an experimental tank: *in* Cornell University Library: XI IAMG Conference, arXiv preprint physics/0606234.

Portniaguine, O., and Zhdanov, M.S., 1999, Focusing geophysical inversion images: Geophysics, **64**, 874–887.

Sapia, V., Oldenborger, G.A., Viezzoli, A., and Marchetti, M., 2014, Incorporating ancillary data into the inversion of airborne time-domain electromagnetic data for hydrogeological applications: Journal of Applied Geophysics, **104**, 35–43.

Sapia, V., Viezzoli A., and Oldenborger, G.A., 2015a, Joining multiple AEM datasets to improve accuracy, cross calibration and derived products. The Spiritwood VTEM and AeroTEM case study: Near Surface Geophysics, **12**, 34–46.

Sapia, V., Oldenborger, G.A., Jørgensen, F., Pugin, A.J.M., Marchetti, M., and Viezzoli, A., 2015b, 3D modeling of buried valley geology using airborne electromagnetic data: Interpretation, **3**, SAC9–SAC22.

Schamper, C., Jørgensen, F., Auken, E., and Effersø, F., 2014, Assessment of near-surface mapping capabilities by airborne transient electromagnetic data – An extensive comparison to conventional borehole data: Geophysics, **79**, B187–B199.

Sengpiel, K.P., and Siemon, B., 2000, Advanced inversion methods for airborne electromagnetic exploration: Geophysics, **65**, 1983–1992.

Viezzoli, A., Christiansen, A.V., Auken, E., and Sørensen, K.I., 2008, Quasi-3D modeling of airborne TEM data by Spatially Constrained Inversion: Geophysics, **73**, F105–F113.

Viezzoli, A., Munday, T., Auken, E., and Christiansen, A.V., 2010, Accurate quasi 3D versus practical full 3D inversion of AEM data – the Bookpurnong case study: Preview, **149**, 23–31.

Vignoli, G., and Zanzi, L., 2005, Focusing inversion technique applied to radar tomographic data: *in* Near Surface 2005: 11th European Meeting of Environmental and Engineering Geophysics, 270–275.

Vignoli, G., Deiana, R., and Cassiani, G., 2012, Focused inversion of vertical radar profile (VRP) traveltime data: Geophysics, **77**, H9–H18.

Vignoli, G., Fiandaca, G., Christiansen, A.V., and Auken, E., 2015a, Sharp Spatially Constrained Inversion (sSCI) with applications to transient electromagnetic data: Geophysical Prospecting, **63**, 243–255.

Vignoli, G., Høyer, A.-S., Behroozmand, A.A., and Viezzoli, A., 2015b, Sharp SCI: a new practical tool for blocky models reconstruction: *in* Extended Abstracts: 24th International Geophysical Conference and Exhibition, ASEG, 1–4.

Vignoli, G., Gervasio, I., Brancatelli, G., Boaga, J., Della Vedova, B., and Cassiani, G., 2016, Frequency-dependent multi-offset phase analysis of surface waves: an example of high-resolution characterization of a riparian aquifer: Geophysical Prospecting, **64**, 102–111.

Winter, T.C., Benson, R.D., Engberg, R.A., Wiche, G.J., Emerson, D.G., Crosby, O.A., and Miller, J.E., 1984, Synopsis of ground-water and surface-water resources of North Dakota: *in* United States Geological Survey, Open File Report, 84–732.

Zhdanov, M.S., Vignoli, G., and Ueda, T., 2006, Sharp boundary inversion in crosswell travel-time tomography: Journal of Geophysics and Engineering, **3**, 122–134.

Zhdanov, M.S., 2009, New advances in regularized inversion of gravity and electromagnetic data, Geophysical Prospecting, **57**, 463–478.